

Supporting information

Work Function: A Determining Factor of the Photodegradation Rate of Methyl Orange via Hollow Octadecahedron Cu₂O Crystals

Bo Zhang^{a,‡}, Shaowei Liao^{a,‡}, Wenjun Wu^{b*}, Hui Li^{a*}, Tianrui Ren^{a*}

^a The Key Laboratory of Resource Chemistry of Ministry of Education, The Development Centre of Plant Germplasm Resources, College of Life and Environmental Science, Shanghai Normal University, 100 Guilin Road, Shanghai, 200234, P. R. China

^b Key Laboratory for Advanced Materials and Institute of Fine Chemicals, Shanghai Key Laboratory of Functional Materials Chemistry, School of Chemistry and Molecular Engineering, East China University of Science and Technology, 130 Meilong Road, Shanghai, 200237, P. R. China

‡ These two authors contributed equally to this work and should be considered co-first authors.

* Corresponding author: Prof. Tianrui Ren

Phone: +86 21 64328850; Fax: +86 21 64328850; E-mail address: trren@shnu.edu.cn

Prof. Hui Li

Phone: +86 21 64323578; Fax: +86 21 64323578; E-mail address: lihui@shnu.edu.cn

Prof. Wenjun Wu

Phone: +86 21 64250940; Fax: +86 21 64252288; E-mail address: wjwu@ecust.edu.cn

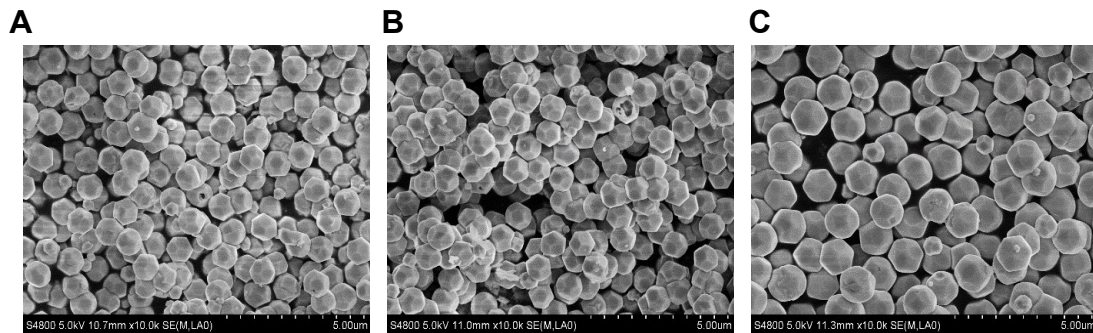


Figure S1. FESEM images of (a) HO-1, (b) HO-2 and (c) HO-3.

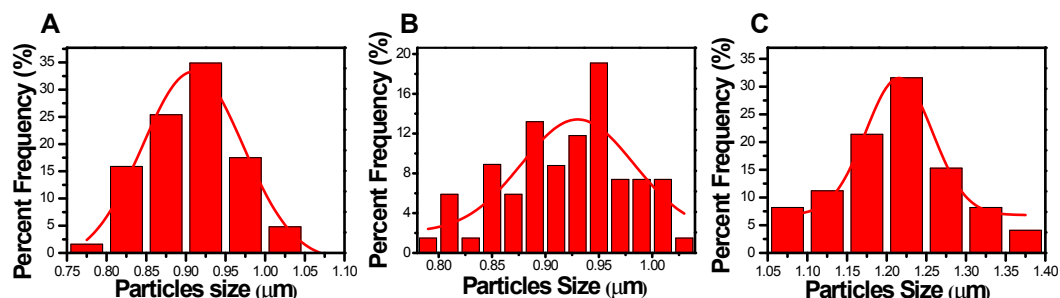


Figure S2. Size distribution histograms for HO-1, HO-2 and HO-3.

Table S1. Average particle sizes and relative standard deviations of the Cu₂O nanocrystals synthesized.

Sample	Average	Relative
	Particle Size (nm)	Standard Deviation (%)
HO-1	910 ± 4.8	0.53
HO-2	930 ± 10	1.11
HO-3	1220 ± 5.4	0.44

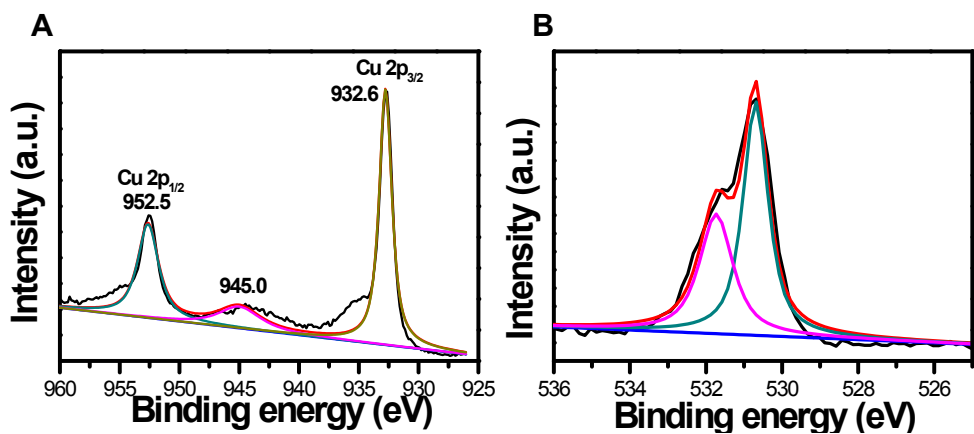


Figure S3. The high resolution XPS spectrum of Cu 2p (A) and O 1s (B) of **HO-1**.

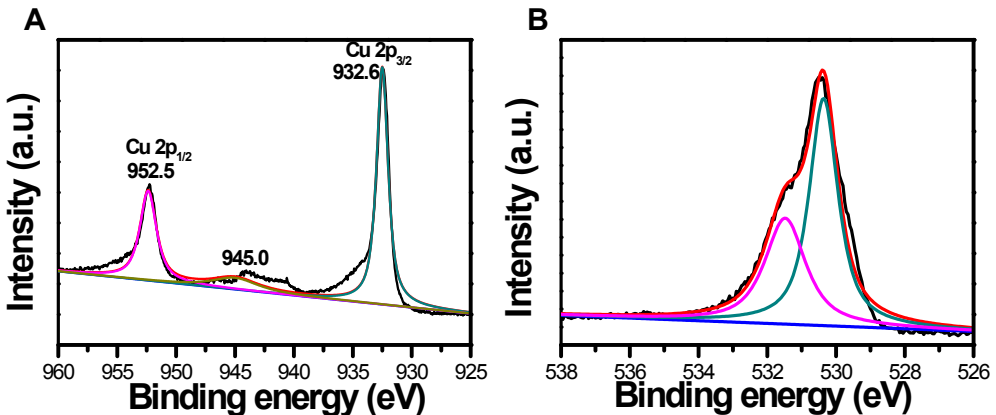


Figure S4. The high resolution XPS spectrum of Cu 2p (A) and O 1s (B) of **HO-3**.

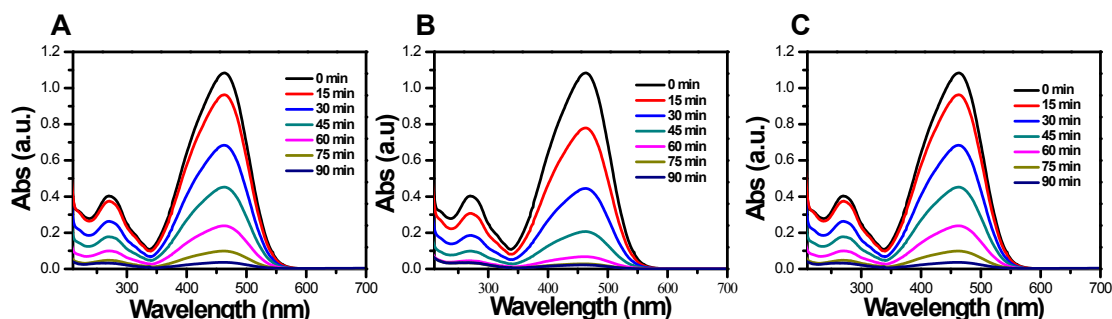


Figure S5. UV-vis absorption spectra of 15 mg/L MO solution as a function of irradiation time using (a) **HO-1**, (b) **HO-2** and **HO-3**.

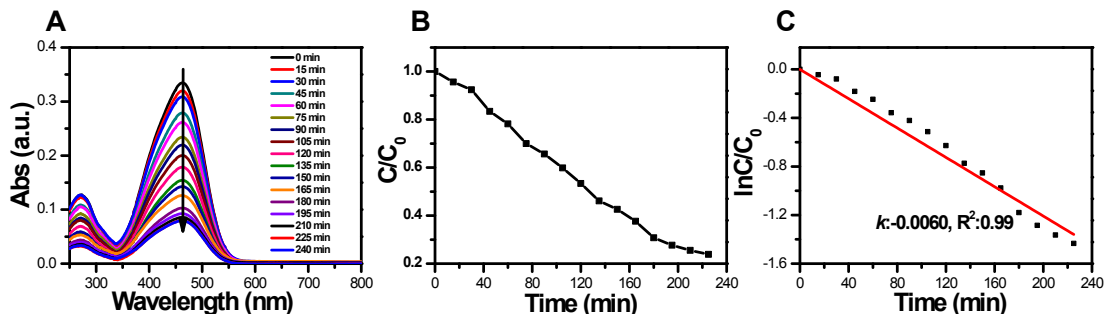


Figure S6. (A) UV-vis absorption spectra of 50 mg/L MO solution as a function of irradiation time using **HO-2**. (B) Extent of photodegradation of 50 mg/L MO solution vs time using **HO-2** as the photocatalysts. (C) Kinetic plots of the degradation process under visible light with **HO-2**.

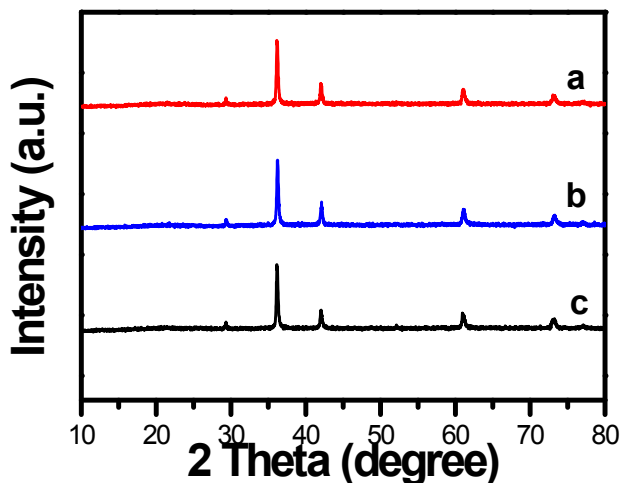


Figure S7. XRD patterns of (a) HO-1, (b) HO-2, and (c) HO-3 after photocatalytic degradation for three cycles.

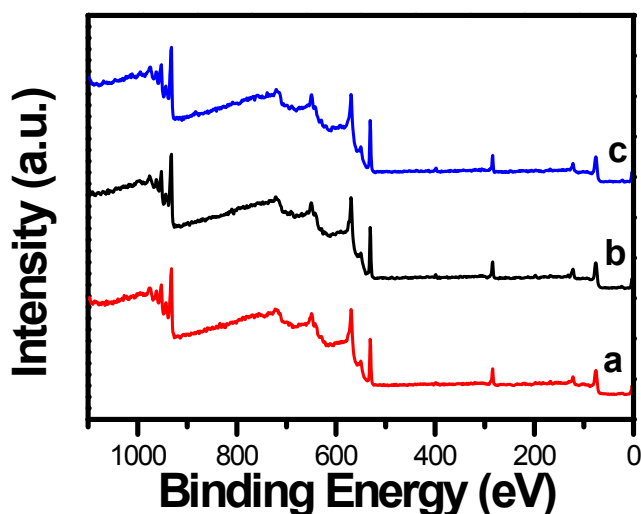


Figure S8. XPS patterns of (a) HO-1, (b) HO-2 and (c) HO-3 after photocatalytic degradation for three cycles.

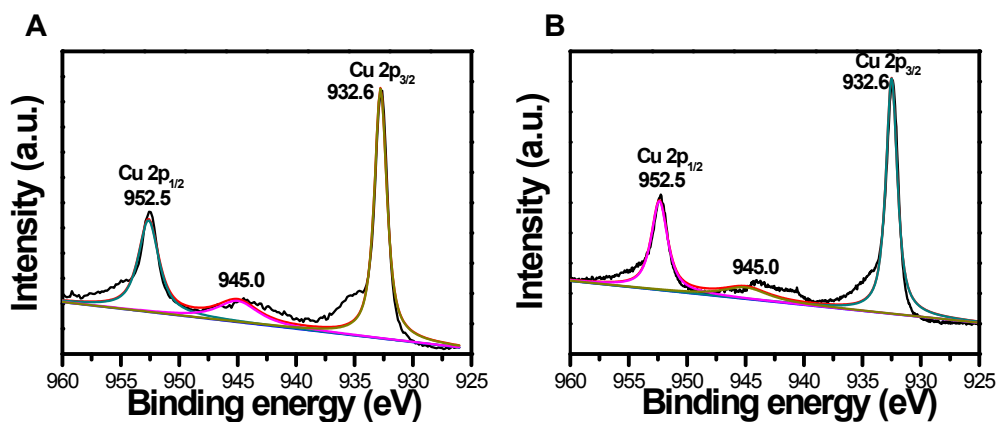


Figure S9. High resolution Cu 2p XPS spectrum of (A) HO-1 and (B) HO-3 after photocatalytic degradation for three cycles

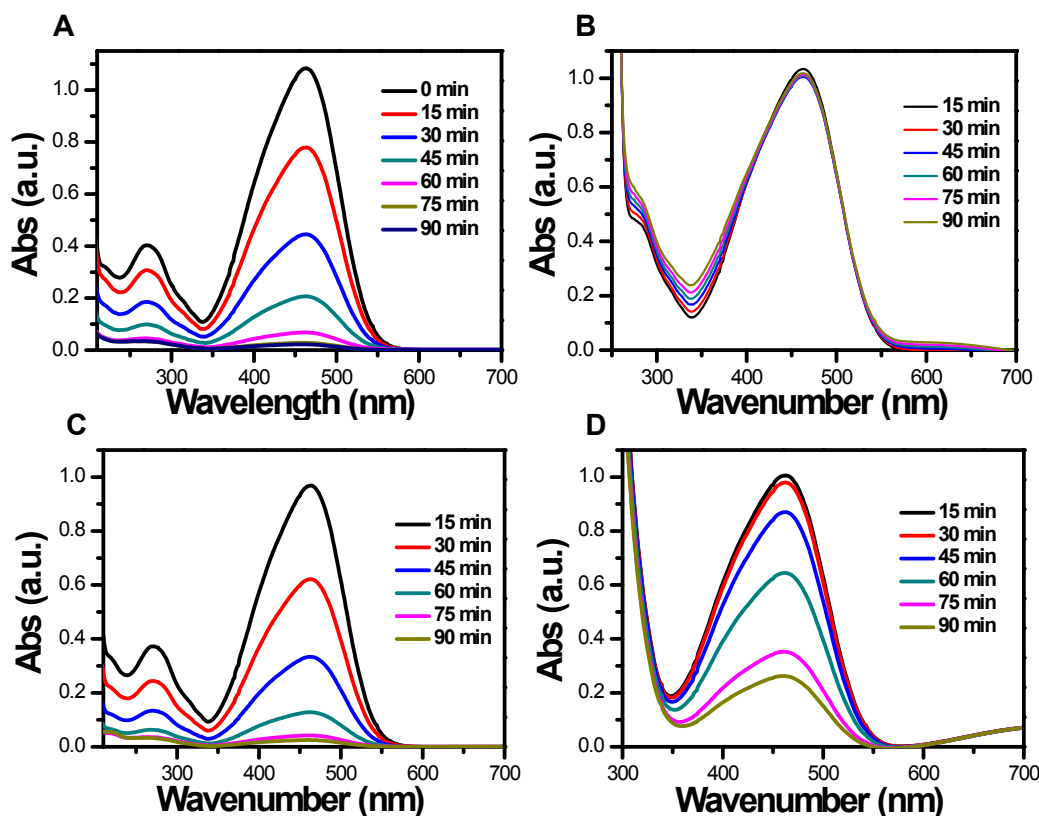


Figure S10. Photocatalytic degradation of MO with **HO-2** in the absence of scavenger (A) and in the presence of p-benzoquinone (B), TBA (C) and EDTA-2Na (D) as scavengers under visible light irradiation.

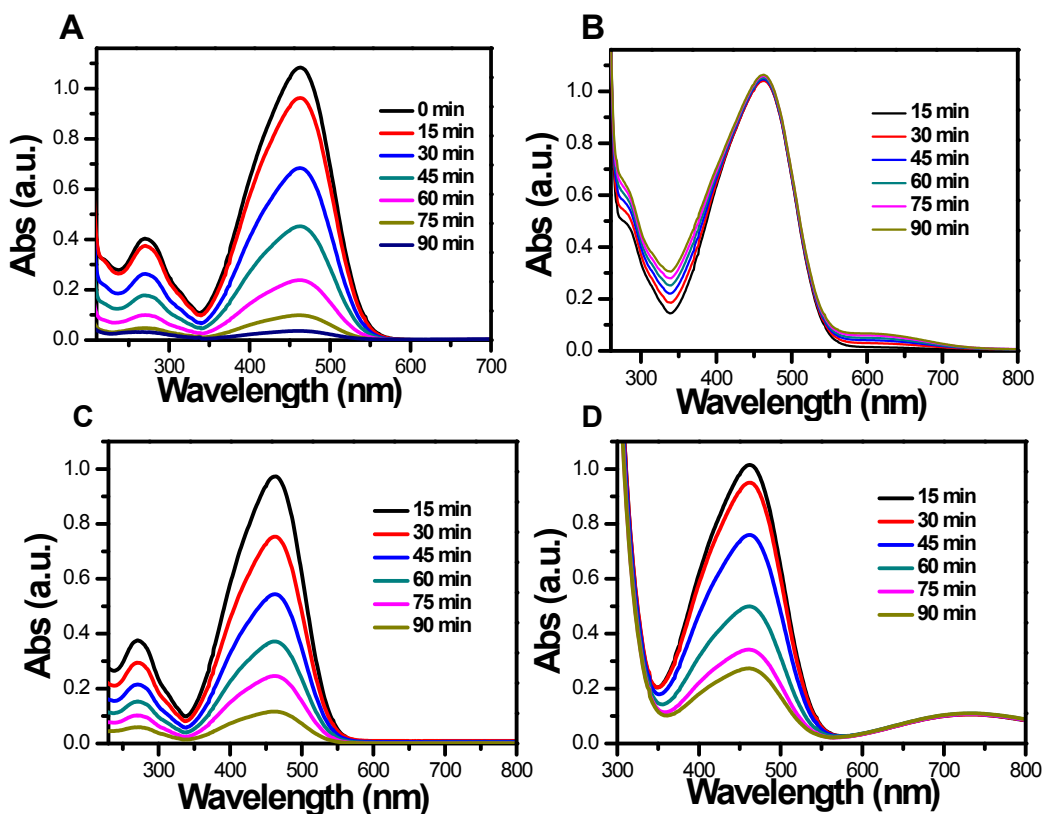


Figure S11. Photocatalytic degradation of MO with **HO-1** in the absence of scavenger (A) and in the presence of p-benzoquinone (B), TBA (C) and EDTA-2Na (D) as scavengers under visible light irradiation

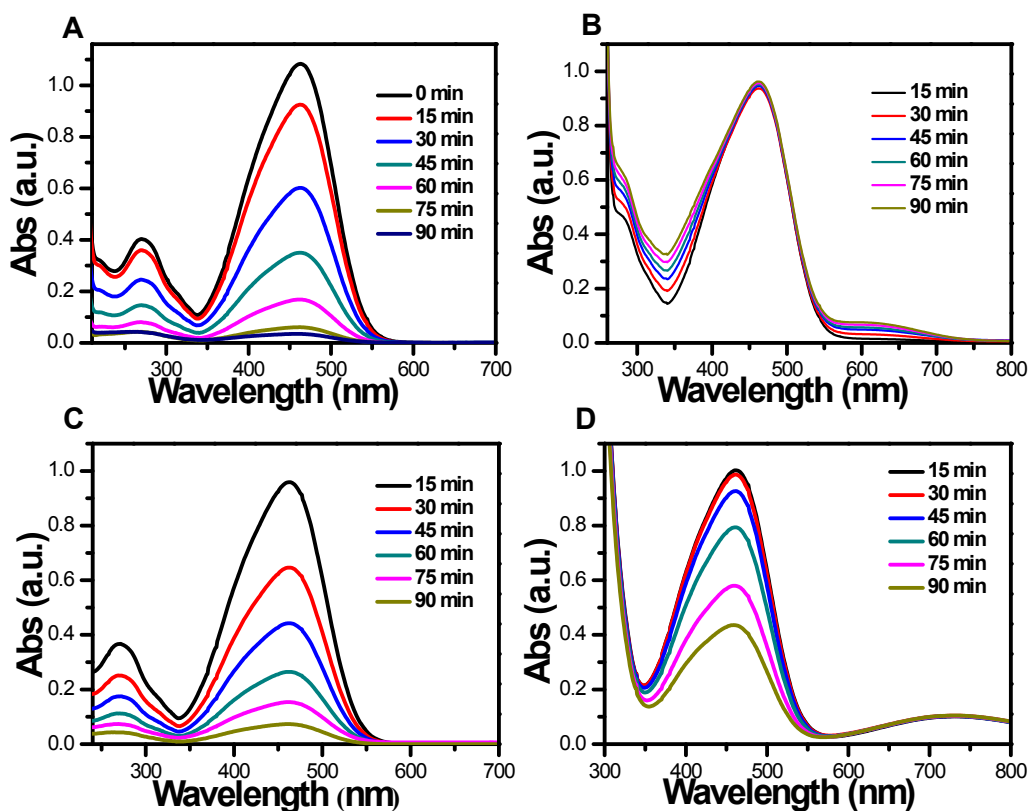


Figure S12. Photocatalytic degradation of MO with **HO-3** in the absence of scavenger (A) and in the presence of p-benzoquinone (B), TBA (C) and EDTA-2Na (D) as scavengers under visible light irradiation.

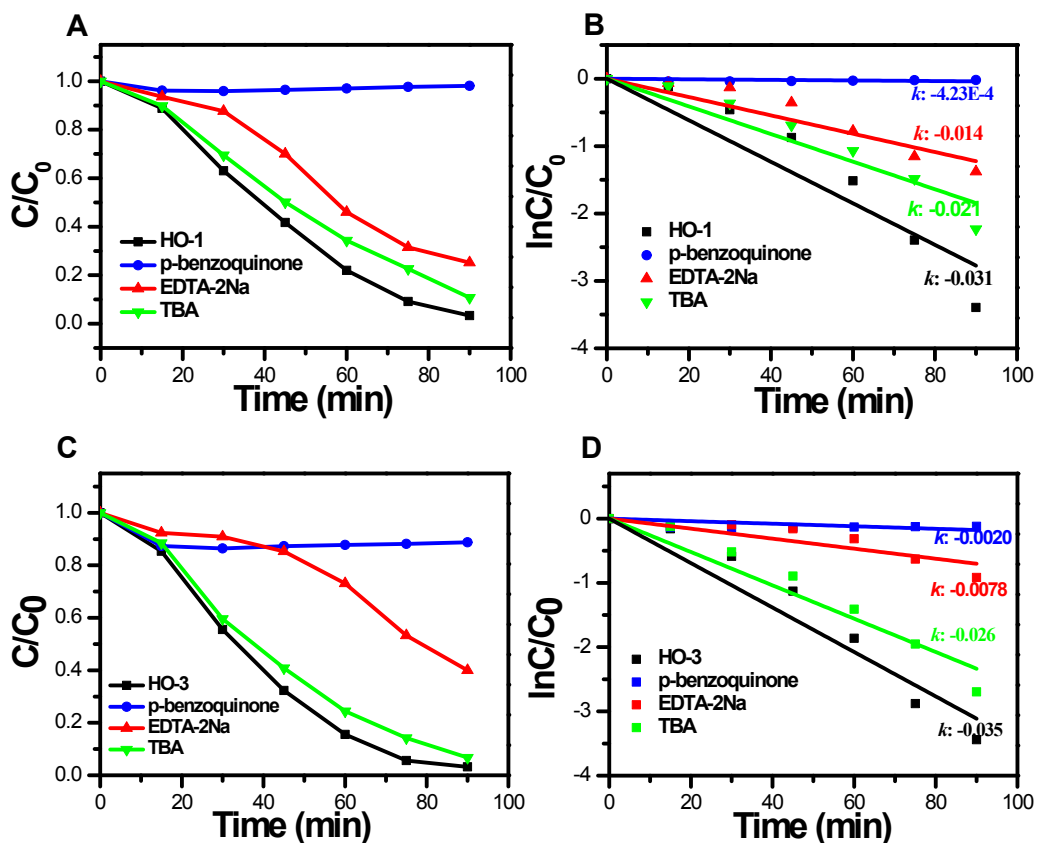


Figure S13. Photocatalytic degradation of MO with **HO-1** (A) and **HO-3** (C) in the absence of scavenger and in the presence of EDTA-2Na, p-benzoquinone and TBA as scavengers under visible light irradiation. Kinetic plots of the degradation process under visible light with **HO-1** (B), and **HO-3** (D). The corresponding first-order linear regressions and apparent reaction rates k were also obtained.

